Behavior of nine levels NPC three-phase inverter topology interfacing photovoltaic system to the medium electric grid under variable irradiance

Rabiaa Mechouma, Hamza Mebarki & Boubekeur Azoui

Electrical Engineering
Archiv für Elektrotechnik

ISSN 0948-7921
Volume 100
Number 3

Electr Eng (2018) 100:2129-2145
DOI 10.1007/s00202-018-0687-7

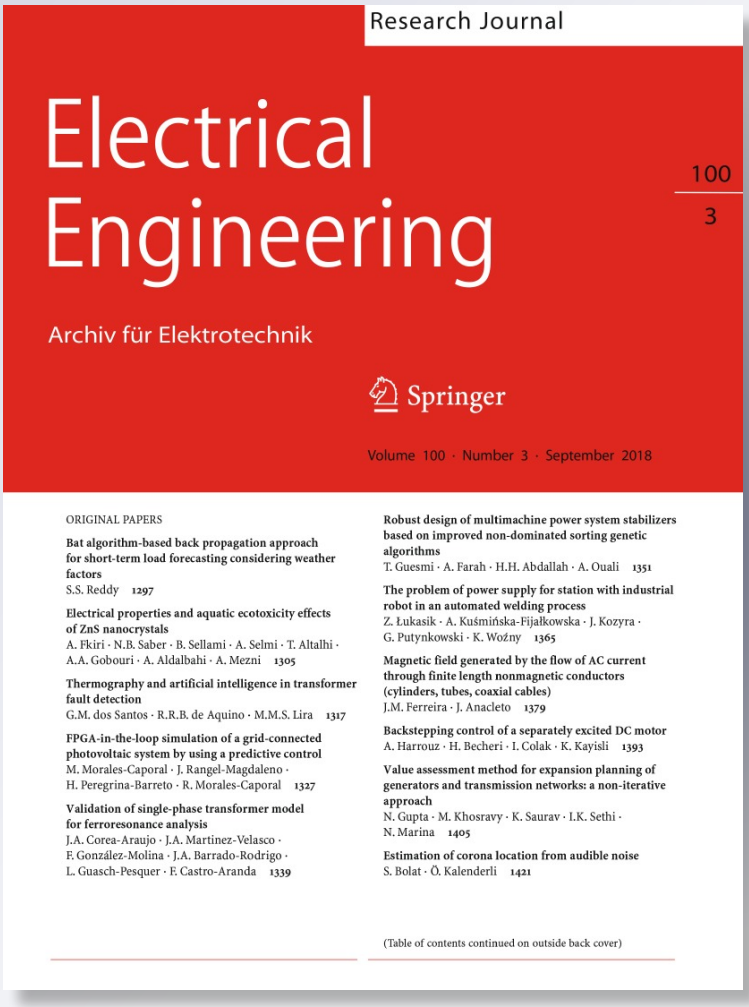

Springer

Your article is protected by copyright and all rights are held exclusively by Springer-Verlag GmbH Germany, part of Springer Nature. This e-offprint is for personal use only and shall not be self-archived in electronic repositories. If you wish to self-archive your article, please use the accepted manuscript version for posting on your own website. You may further deposit the accepted manuscript version in any repository, provided it is only made publicly available 12 months after official publication or later and provided acknowledgement is given to the original source of publication and a link is inserted to the published article on Springer's website. The link must be accompanied by the following text: "The final publication is available at link.springer.com".

Author's personal copy

Electrical Engineering (2018) 100:2129–2145
https://doi.org/10.1007/s00202-018-0687-7

ORIGINAL PAPER

Behavior of nine levels NPC three-phase inverter topology interfacing photovoltaic system to the medium electric grid under variable irradiance

Rabiaa Mechouma[1] · Hamza Mebarki[1] · Boubekeur Azoui[1]

Received: 18 April 2017 / Accepted: 17 March 2018 / Published online: 27 March 2018
© Springer-Verlag GmbH Germany, part of Springer Nature 2018

Abstract
To reach the increasing demand for power quality and power rating along with lower harmonic distortion and lesser electromagnetic interference, the multilevel inverter is needed. Solar energy is one of the favorable renewable energy resources, and the multilevel inverter has been proven to be one of the important enabling technologies in photovoltaic utilization. This paper is based on the study of behavior of a nine levels NPC three-phase inverter topology interfacing multistring photovoltaic system to the electric grid. This inverter is controlled by the pulse-width modulated strategy. Eight carrier waves of the same frequency and different amplitudes are compared with two references (a sine wave and its opposite) for generating the control signals of the switches. Some DC/DC boost converters are used to amplify the voltage produced by the photovoltaic generators. Each of these converters is controlled by a fuzzy Logic-based maximum power point tracking algorithm (FLBMPPTA) in order to track the maximum power point of the GPV; results of simulation in Matlab environment are given and discussed.

Keywords Grid-connected photovoltaic system (GCPVS) · Multilevel three-phase NPC multistring inverter · Multicarrier PWM · Fuzzy logic control · Medium voltage grid

1 Introduction

A multilevel inverter is a power electronic device built to synthesize a desired AC voltage from several levels of DC voltages. Such inverters have been the subject of research in the last several years where the DC levels were considered to be identical in that all of them were capacitors, batteries, solar cells, etc. [1]. It has gained much attention due to its advantages in lower switching loss, better electromagnetic compatibility, higher voltage capability and lower harmonics. Multilevel inverters include an array of power semiconductors and capacitor voltage sources, the output of which generate voltages with stepped waveforms. The commutation of the switches permits the addition of the capacitor voltages, which reach high voltage at the output, while the power semiconductors must withstand only reduced voltages. Photovoltaic (PV), wind energy, and hydro-conversion are the most explored technologies due to their considerable advantages [2,3], such as reliability, reasonable installation and energy production costs, low environmental impact, possibility to support micro grid systems and to connect to the electric grid [4]. In this paper, we present a multicarrier dual reference very low frequency three-phase neutral point clamped (NPC) inverter designed for photovoltaic system connected to a medium voltage grid. This inverter is controlled by a pulse-width modulated (PWM) strategy based on the comparison of several carrier waves with two reference signals, so more control signals are obtained. Instead of a single photovoltaic generator at the input of the inverter, we have a multiple continuous source which is composed of several photovoltaic generators. Each of them consists of N_P branches, each of which is composed of N_S solar panels in series. Each generator of this source generates a voltage which is amplified at the output by means of a dc/dc converter. This converter is controlled by a fuzzy logic-based maximum power point tracking algorithm (FLBMPPTA). The overall system is shown in Fig. 1. The study is simulated in Matlab/Simulink, and results are given and discussed.

✉ Rabiaa Mechouma
rabiaa.mechouma@yahoo.com

[1] LEB, University of Batna 2, Avenue Chahid Boukhlouf Mohammed Elhadi, 05001 Batna, Algérie

Author's personal copy

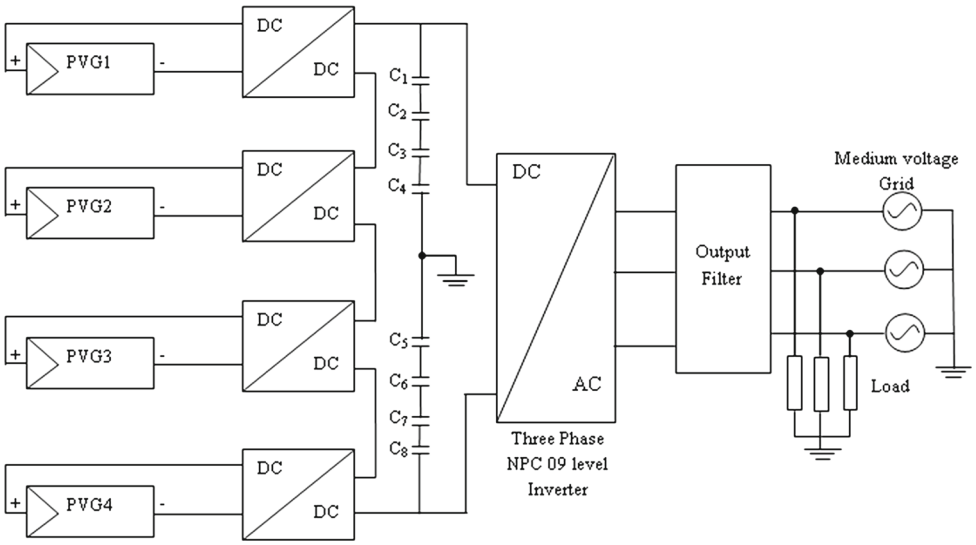

Fig. 1 Schematic diagram of the overall PV system

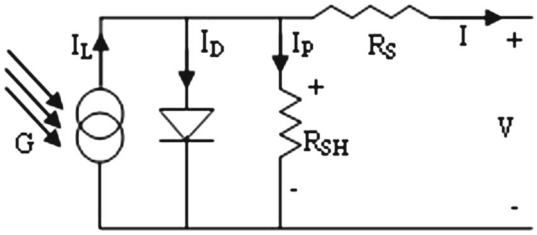

Fig. 2 Equivalent circuit diagram of a PV cell

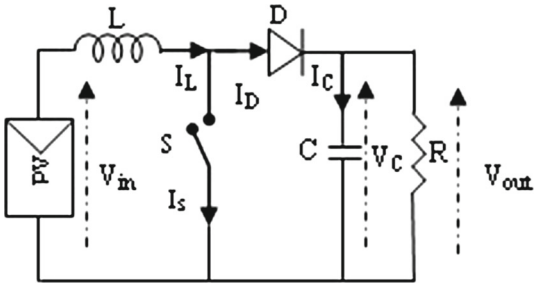

Fig. 3 Boost converter schematic

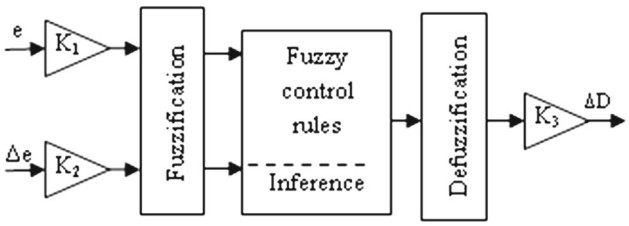

Fig. 4 Basic structure of fuzzy logic control

2 Modeling of the global grid-connected photovoltaic system structure

Modeling the photovoltaic system is required as a crucial step to describe the functioning of all the elements that are all starting from the DC source and are arriving to the grid. It predicts the conceptual and energy performance of PV systems connected to the grid in different climatic conditions and under well-defined loads. Models of the various components will be presented as follows:

2.1 The photovoltaic source model

As already mentioned, the photovoltaic source consists of 04 parts, each of them represents a partial photovoltaic generator. Each partial PVG generates at its output a DC voltage which is then amplified by a DC/DC converter. Continuous output voltages of the converters are then summed to obtain an overall voltage that feeds the inverter. The equivalent circuit diagram of a PV cell is illustrated in Fig. 2.

The selected model in this work is inspired from references [5–7]. The advantage of this model can be established using only standard data for the module and cells provided by the manufacturer in the technical data (data and graphs). It is independent of the saturation current I_S of the diode (see Fig. 2). Assuming R_{SH} as infinite and its branch becomes an open circuit, the current supplied by the solar module (I_M) in any condition is given by:

$$I_M = I_{SCM}\left[\frac{I_{PH}}{I_{SCM}} - \left\{\exp\left(\frac{V_M - V_{OCM} + I_M R_{SM}}{n V_{THM}}\right) - \exp\left(\frac{-V_{OCM}}{n V_{THM}}\right)\right\}\right] \quad (1)$$

where I_{SCM} and V_{OCM} are, respectively, the short-circuit current and the open-circuit voltage of the solar module at the standard test conditions (STC), I_M and V_M are, respectively, the current and the voltage delivered by the solar module in any condition, R_{SM} is the series resistance of the solar mod-

Author's personal copy

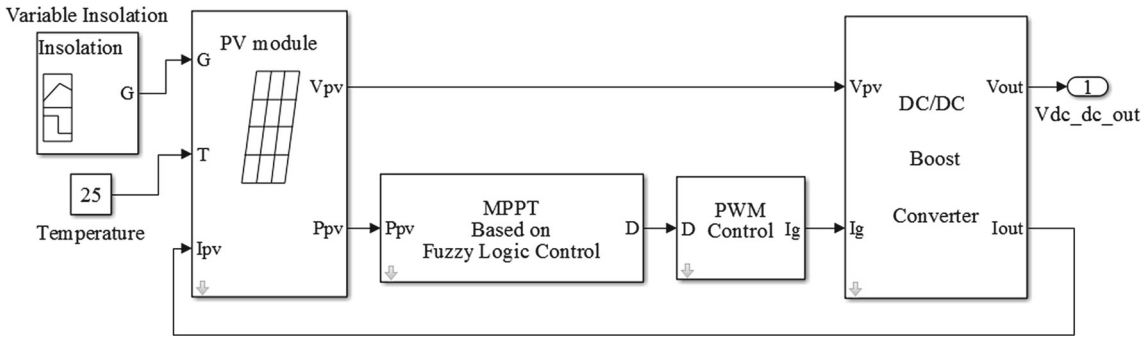

Fig. 5 Simulation scheme of one partial (PV) system

Fig. 6 Fuzzy logic MPPT

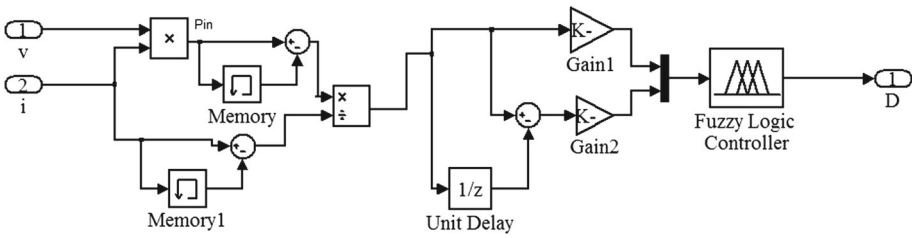

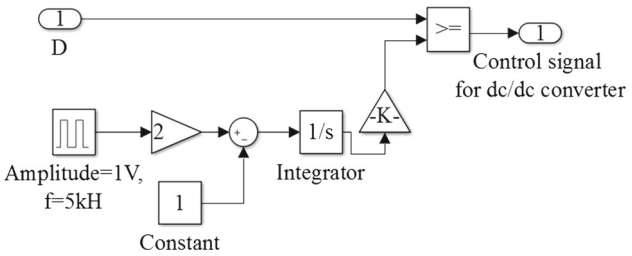

Fig. 7 PWM control

ule, V_{THM} is the thermal voltage of the solar module, and n is the quality factor which varies typically from 1 to 2.

V_{OCM} and I_{SCM} are given by:

$$V_{\mathrm{OCM}} = V_{\mathrm{OCC}} \times N_{\mathrm{SC}} \tag{2}$$

$$I_{\mathrm{SCM}} = I_{\mathrm{SCC}} \times N_{\mathrm{PC}} \tag{3}$$

where I_{SCC} and V_{OCC} are, respectively, the short-circuit current and the open-circuit voltage of the solar cell at the standard test conditions (STC), N_{PC} and N_{SC} are, respectively, the number of branches of cells in parallel in the solar module and the number of cells in series in each branch.

The thermal voltage of the solar module is given by:

$$V_{\mathrm{THM}} = V_{\mathrm{THC}} \times N_{\mathrm{SC}} \tag{4}$$

where $V_{\mathrm{THC}} = \frac{KT_{\mathrm{C}}}{q}$, which is the thermal voltage of the solar cell.

The series resistance of the module is given by:

$$R_{\mathrm{SM}} = \frac{N_{\mathrm{SC}}}{N_{\mathrm{PC}}} R_{\mathrm{SC}} \tag{5}$$

where V_{THC} is the thermal voltage of the PV cell, R_{SC} is the series resistance of the PV cell, K is the Boltzmann's constant ($K = 1.38 \times 10^{-23}\,\mathrm{m^2 kg\,s^{-2}\,K^{-1}}$), and q is the electrical charge of the electron ($q = 1.6 \times 10^{-19}$ coulombs).

The open-circuit voltage of the PV cell is given by:

$$V_{\mathrm{OCC}} = V_{\mathrm{OCC-ref}} + \beta\,(T - T_{\mathrm{ref}}) \tag{6}$$

where $V_{\mathrm{OCC-ref}}$ is the open-circuit voltage of the PV cell in standard conditions, T_{ref} is the reference value of the temperature ($T_{\mathrm{ref}} = 25\,^{\circ}\mathrm{C}$), and β represents the temperature coefficient of the short-circuit current (%/°K).

The thermal voltage of the PV cell can be easily calculated using the coordinates of the maximum power point of the cell (V_{MPPC} and I_{MPPC}). The expression of V_{THC} is:

$$V_{\mathrm{THC}} = \frac{V_{\mathrm{MPPC}} + R_{\mathrm{SC}} I_{\mathrm{MPPC}} - V_{\mathrm{OCC}}}{\mathrm{Ln}\left(1 - \frac{I_{\mathrm{MPPC}}}{I_{\mathrm{SCC}}}\right)} \tag{7}$$

The current delivered by each PVG is given by the following expression:

$$I_{\mathrm{M}} = N_{\mathrm{P}} I_{\mathrm{SCM}} \left[\frac{I_{\mathrm{PH}}}{I_{\mathrm{SCM}}} - \left\{\exp\left(\frac{N_{\mathrm{S}} V_{\mathrm{M}} - N_{\mathrm{S}} V_{\mathrm{OCM}} + N_{\mathrm{P}} I_{\mathrm{M}} R_{\mathrm{SM}}}{n N_{\mathrm{S}} V_{\mathrm{THM}}}\right) - \exp\left(\frac{-V_{\mathrm{OCM}}}{\mathrm{nN_S} V_{\mathrm{THM}}}\right)\right\}\right] \tag{8}$$

Author's personal copy

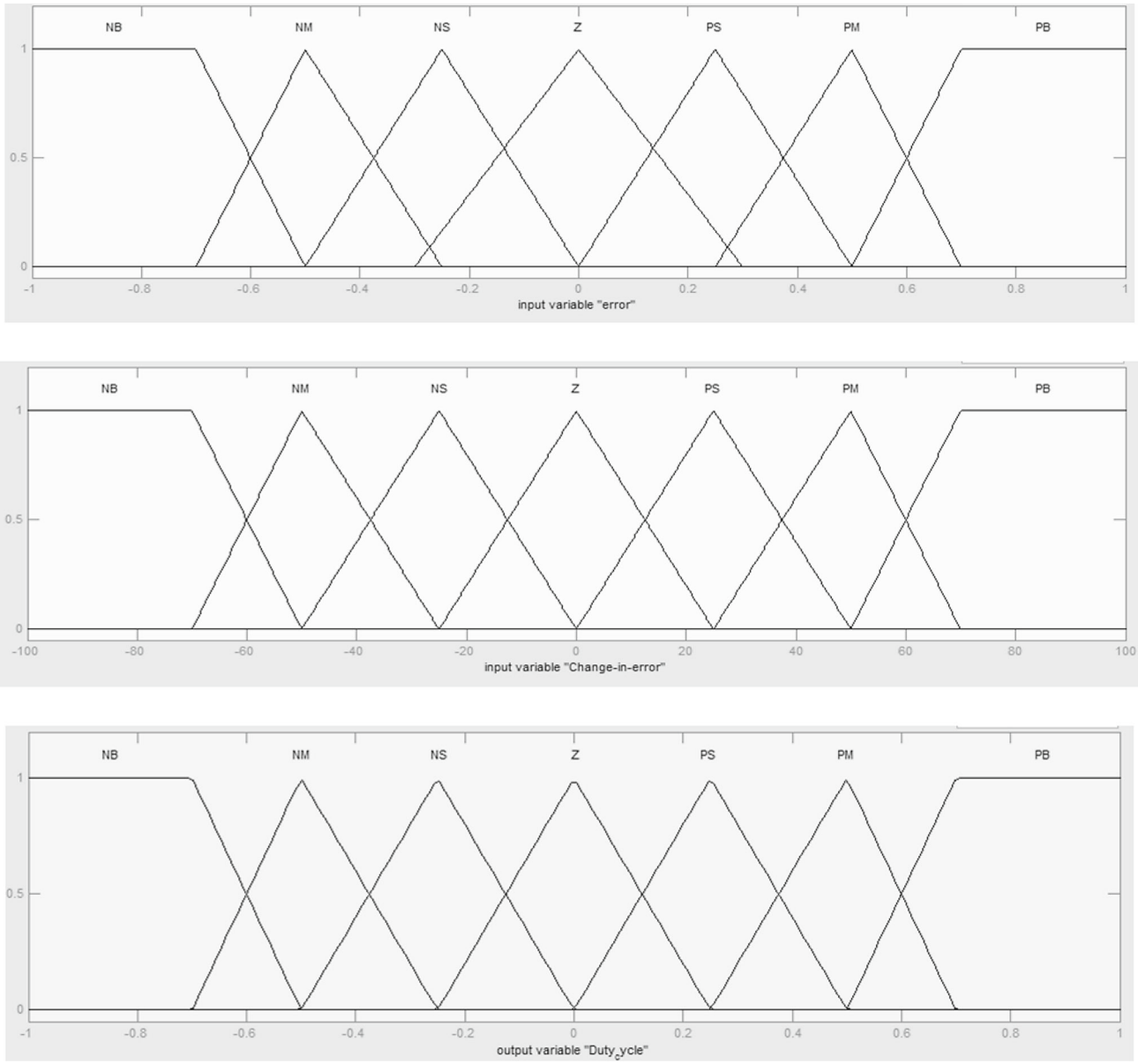

Fig. 8 Membership functions of FLC

2.2 DC/DC boost converter and its control

2.2.1 DC/DC boost converter model

A boost converter (step-up converter) is a DC-to-DC power converter with an output voltage greater than its input voltage. A schematic of a boost power stage is shown in Fig. 3. The basic principle of a boost converter consists of two distinct states.

(a) In the On-state, the switch "S" is closed and the state space model of the DC/DC converter is presented by Eq. (9).

$$\begin{bmatrix} \frac{dI_L}{dt} \\ \frac{dV_C}{dt} \end{bmatrix} = \begin{bmatrix} 0 & 0 \\ 0 & \frac{1}{RC} \end{bmatrix} \begin{bmatrix} I_L \\ V_C \end{bmatrix} + \begin{bmatrix} \frac{1}{L} \\ 0 \end{bmatrix} V_{in} \tag{9}$$

(b) In the OFF-state, the switch "S" is open and the state space model of the DC/DC converter is presented by Eq. (10).

$$\begin{bmatrix} \frac{dI_L}{dt} \\ \frac{dV_C}{dt} \end{bmatrix} = \begin{bmatrix} 0 & \frac{-1}{L} \\ \frac{1}{C} & \frac{-1}{RC} \end{bmatrix} \begin{bmatrix} I_L \\ V_C \end{bmatrix} + \begin{bmatrix} \frac{1}{L} \\ 0 \end{bmatrix} V_{in} \tag{10}$$

Author's personal copy

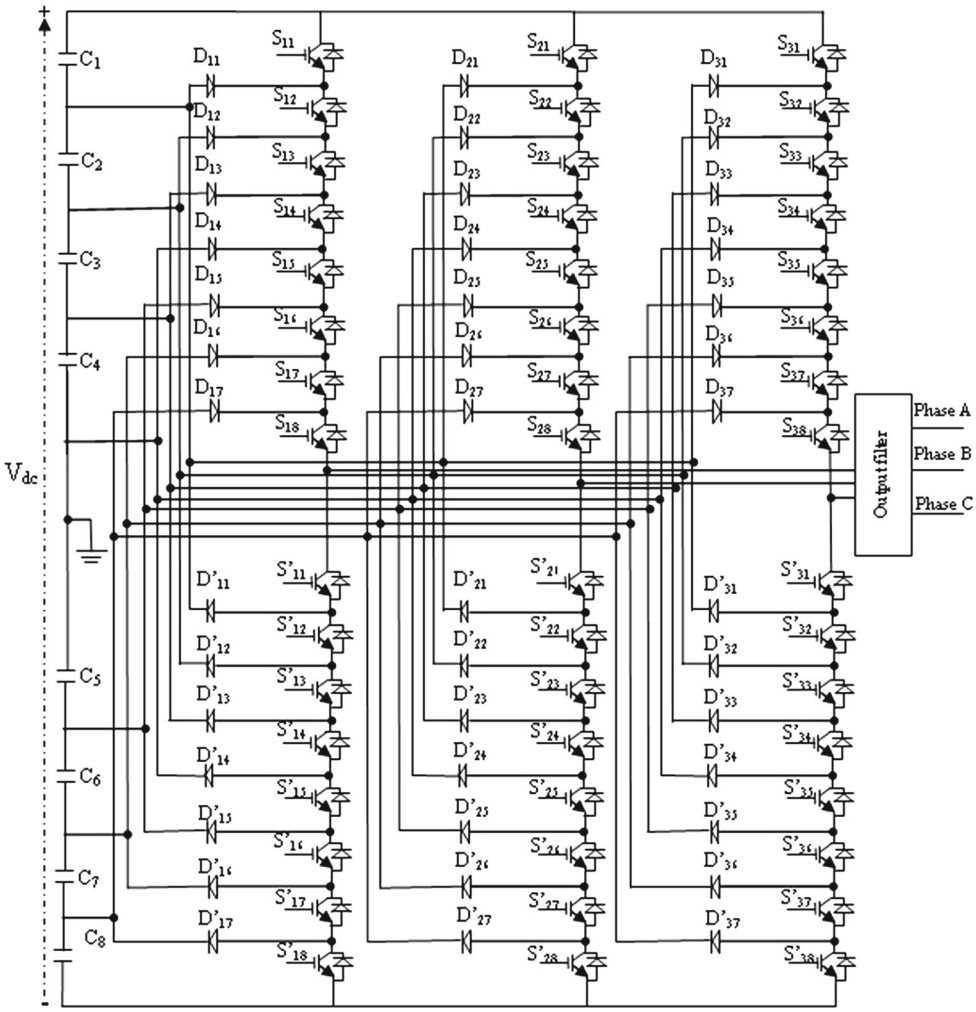

Fig. 9 Diagram of the nine levels NPC three-phase inverter

For a full period of operation (T), the space state model of the dc/dc converter is presented by Eqs. (11) [8].

$$\begin{bmatrix} \frac{dI_L}{dt} \\ \frac{dV_C}{dt} \end{bmatrix} = \left\{ \begin{bmatrix} 0 & 0 \\ 0 & \frac{1}{RC} \end{bmatrix} D + \begin{bmatrix} 0 & \frac{-1}{L} \\ \frac{1}{C} & \frac{-1}{RC} \end{bmatrix} (1-D) \right\} \begin{bmatrix} I_L \\ V_C \end{bmatrix} + \left\{ \begin{bmatrix} \frac{1}{L} \\ 0 \end{bmatrix} D + \begin{bmatrix} \frac{1}{L} \\ 0 \end{bmatrix} (1-D) \right\} V_{in} \quad (11)$$

D is the duty cycle which ranges from 0 ("S" is off) and 1 ("S" is on). We note that the continuous conduction mode is considered for the operation of DC/DC converters.

2.2.2 Fuzzy logic MPPT control

The boost (step-up) DC/DC converter is modeled as a block whose inputs are the voltage delivered by the solar panels and the second input is the duty cycle D generated by the fuzzy logic maximum power point tracking (FLMPPT) controller.

Introduced in 1965 with work of L. Zadeh, fuzzy logic is involved in the handling of imperfect knowledge, and it occurred as an effective alternative for systems of great complexity or unfamiliar design [9]. It permits to define control laws of any process starting from linguistic description of the control strategy to be adopted. Fuzzy logic using controller is a rule-based controller; it consists of an input, processing and output stages [10].

The structure of a process controlled via a fuzzy controller is shown in Fig. 4, which emphasizes the basic components of a fuzzy controller: a fuzzification interface, a knowledge base, a data base, inference procedure, and a defuzzification interface [11].

2.2.3 Simulation of one partial system (photovoltaic generator and DC/DC converter) with MPPT based on fuzzy logic

The schematic of a partial photovoltaic generator connected to the DC/DC boost converter is shown in Fig. 5:

Author's personal copy

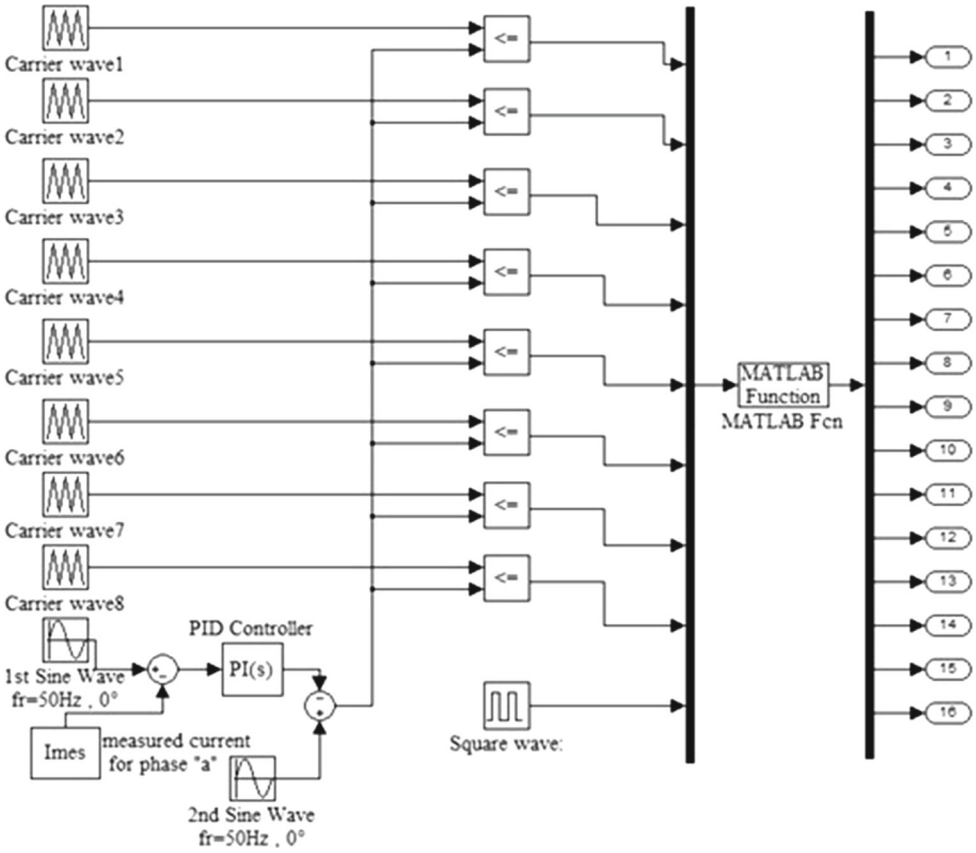

Fig. 10 Control circuit of one arm of the inverter (Phase "a")

Table 1 States of the switches to generate the output voltage "V_a"

The states of the inverter arm switches for phase "a"	The inverter output voltage "V_a" (Volts)
The switches (S_{11}, S_{12}, S_{13}, S_{14}, S_{15}, S_{16}, S_{17}, S_{18}) are closed The switches (S'_{11}, S'_{12}, S'_{13}, S'_{14}, S'_{15}, S'_{16}, S'_{17}, S'_{18}) are open	$\frac{V_{dc}}{2}$
The switches (S_{11}, S_{12}, S_{13}, S_{14}, S_{15}, S_{16}, S_{17}, S'_{18}) are closed The switches (S'_{11}, S'_{12}, S'_{13}, S'_{14}, S'_{15}, S'_{16}, S'_{17}, S_{18}) are open	$\frac{3}{4}\frac{V_{dc}}{2}$
The switches (S_{11}, S_{12}, S_{13}, S_{14}, S_{15}, S_{16}, S'_{17}, S'_{18}) are closed The switches (S'_{11}, S'_{12}, S'_{13}, S'_{14}, S'_{15}, S'_{16}, S_{17}, S_{18}) are open	$\frac{1}{2}\frac{V_{dc}}{2}$
The switches (S_{11}, S_{12}, S_{13}, S_{14}, S_{15}, S'_{16}, S'_{17}, S'_{18}) are closed The switches (S'_{11}, S'_{12}, S'_{13}, S'_{14}, S'_{15}, S_{16}, S_{17}, S_{18}) are open	$\frac{1}{4}\frac{V_{dc}}{2}$
The switches (S_{11}, S_{12}, S_{13}, S_{14}, S'_{15}, S'_{16}, S'_{17}, S'_{18}) are closed The switches (S'_{11}, S'_{12}, S'_{13}, S'_{14}, S_{15}, S_{16}, S_{17}, S_{18}) are open	0
The switches (S_{11}, S_{12}, S_{13}, S'_{14}, S'_{15}, S'_{16}, S'_{17}, S'_{18}) are closed The switches (S'_{11}, S'_{12}, S'_{13}, S_{14}, S_{15}, S_{16}, S_{17}, S_{18}) are open	$\frac{-1}{4}\frac{V_{dc}}{2}$
The switches (S_{11}, S_{12}, S'_{13}, S'_{14}, S'_{15}, S'_{16}, S'_{17}, S'_{18}) are closed The switches (S'_{11}, S'_{12}, S_{13}, S_{14}, S_{15}, S_{16}, S_{17}, S_{18}) are open	$\frac{-1}{2}\frac{V_{dc}}{2}$
The switches (S_{11}, S'_{12}, S'_{13}, S'_{14}, S'_{15}, S'_{16}, S'_{17}, S'_{18}) are closed The switches (S'_{11}, S_{12}, S_{13}, S_{14}, S_{15}, S_{16}, S_{17}, S_{18}) are open	$\frac{-3}{4}\frac{V_{dc}}{2}$
The switches (S'_{11}, S'_{12}, S'_{13}, S'_{14}, S'_{15}, S'_{16}, S'_{17}, S'_{18}) are closed The switches (S_{11}, S_{12}, S_{13}, S_{14}, S_{15}, S_{16}, S_{17}, S_{18}) are open	$-\frac{V_{dc}}{2}$

Author's personal copy

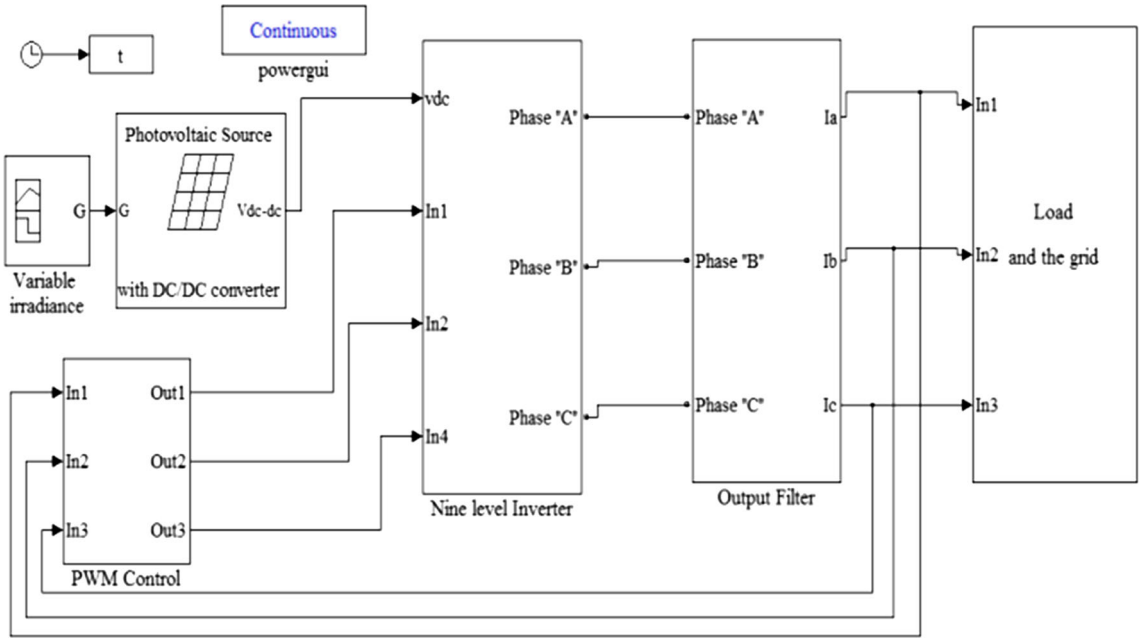

Fig. 11 Simulation scheme of the overall system

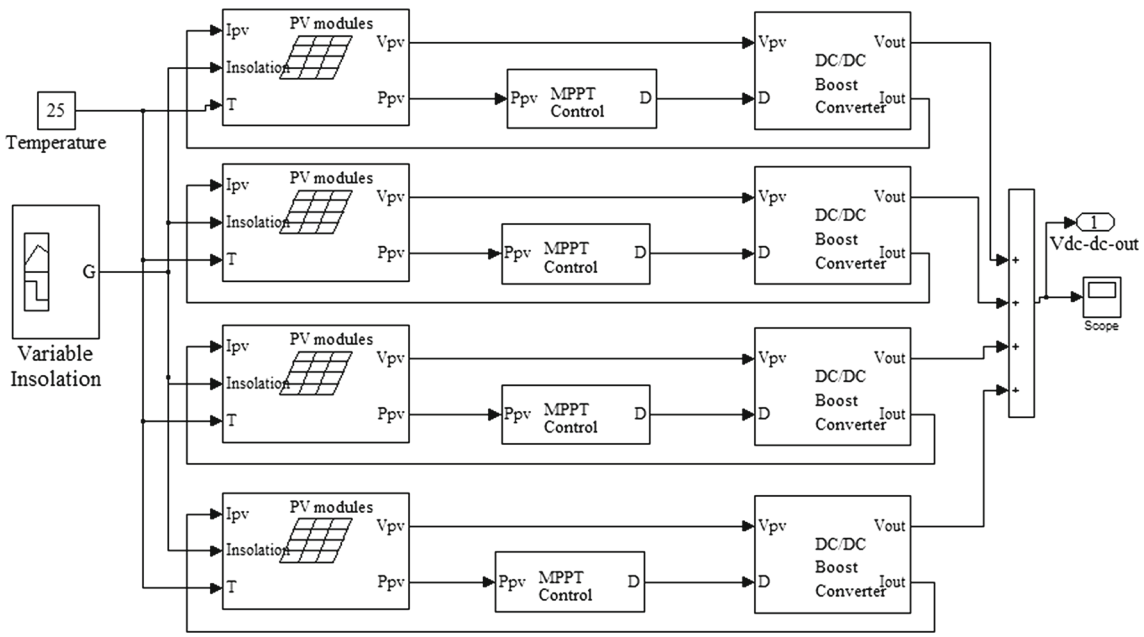

Fig. 12 Overall structure of the PV source with DC/DC converters

The MPPT controller based on fuzzy logic is shown in Fig. 6.

The inputs to a MPPT fuzzy logic controller are error "e" and "Δe" defined by:

$$e(k) = \frac{P(k) - P(k-1)}{I(k) - I(k-1)} \tag{12}$$

$$\Delta e(k) = e(k) - e(k-1) \tag{13}$$

where "e" is the error, "Δ e" change in error, "k" is the discrete-time index, P(k) is the instantaneous power of the PVG, and I(k) is the corresponding instantaneous current. The output variable is the duty cycle D, which is transmitted to the boost DC/DC converter. The MPPT control is followed by the well-known PWM control which is described in Fig. 7.

Author's personal copy

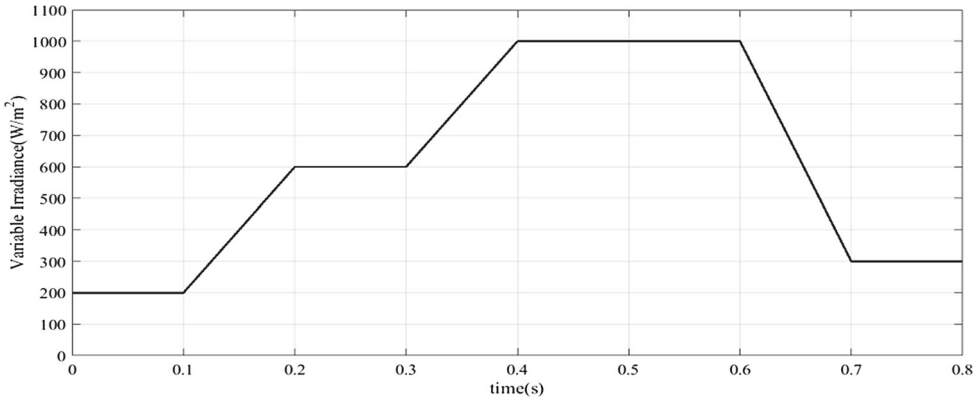

Fig. 13 Variable solar irradiance

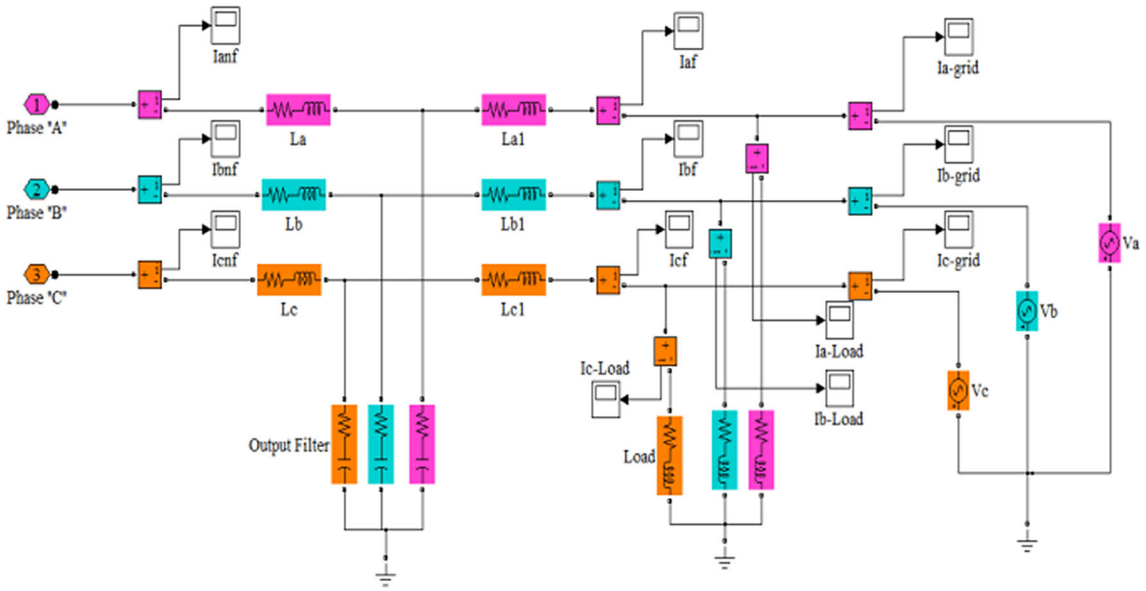

Fig. 14 Output filter, the load, and the grid

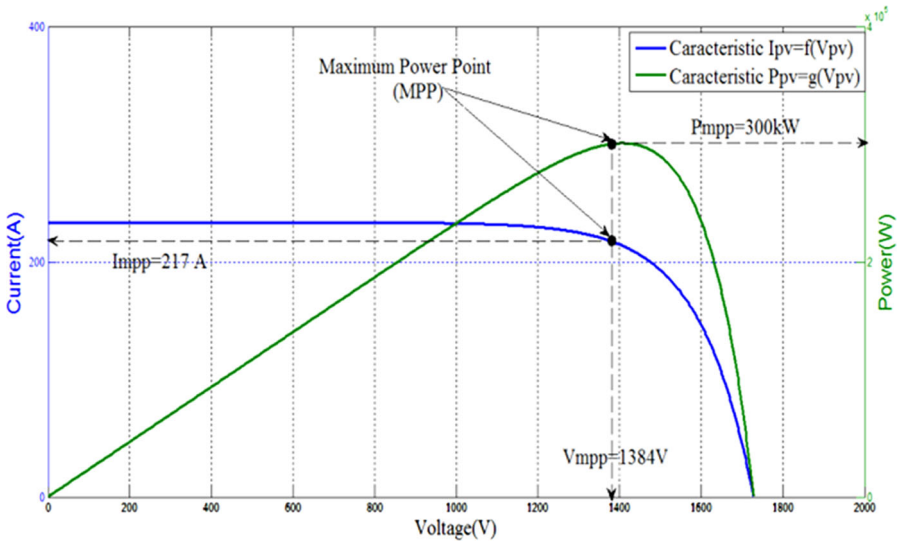

Fig. 15 Characteristics of each photovoltaic generator under standard test conditions (STC): $G = 1000\,\mathrm{W/m^2}$ and $T = 25\,^{\circ}\mathrm{C}$

Author's personal copy

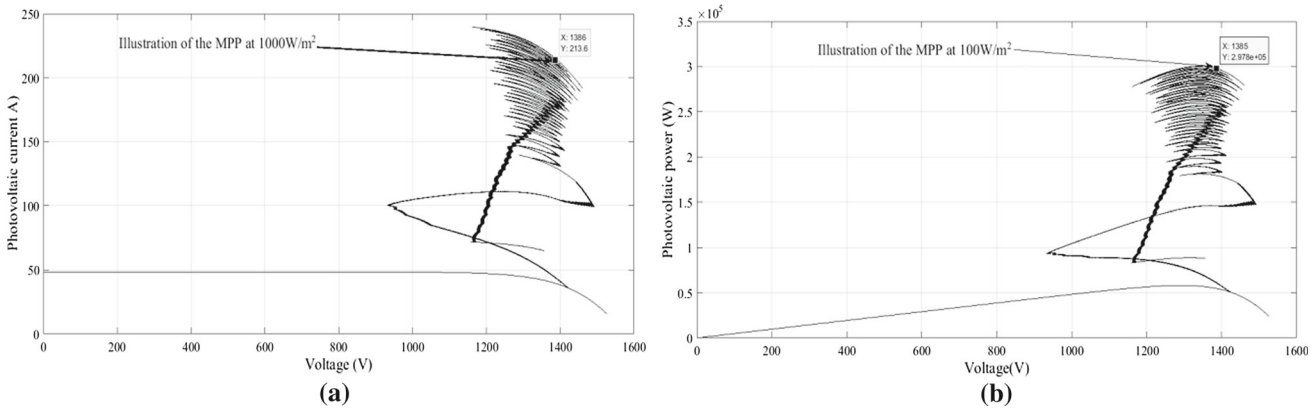

Fig. 16 Characteristics of each photovoltaic generator with MPPT under a variable solar radiation. **a** Current characteristic, **b** power characteristic

Fig. 17 DC/DC converter input and output voltage for each part

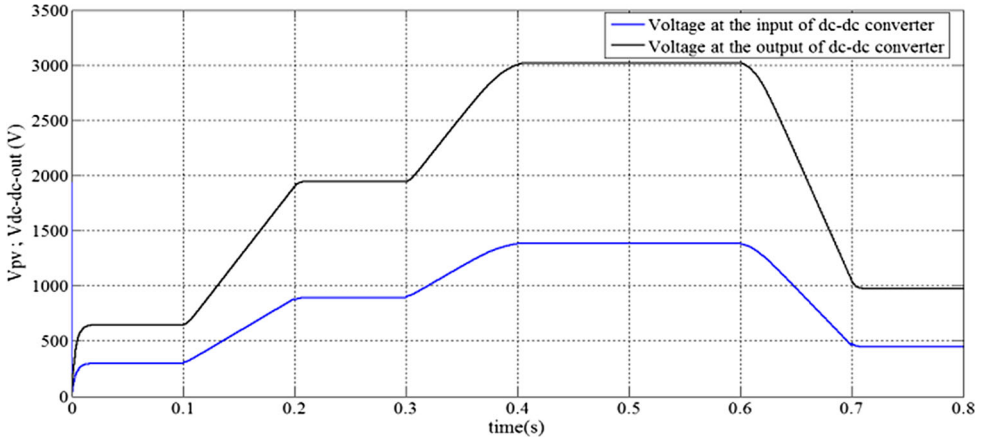

Fig. 18 DC/DC converter input and output power for each part

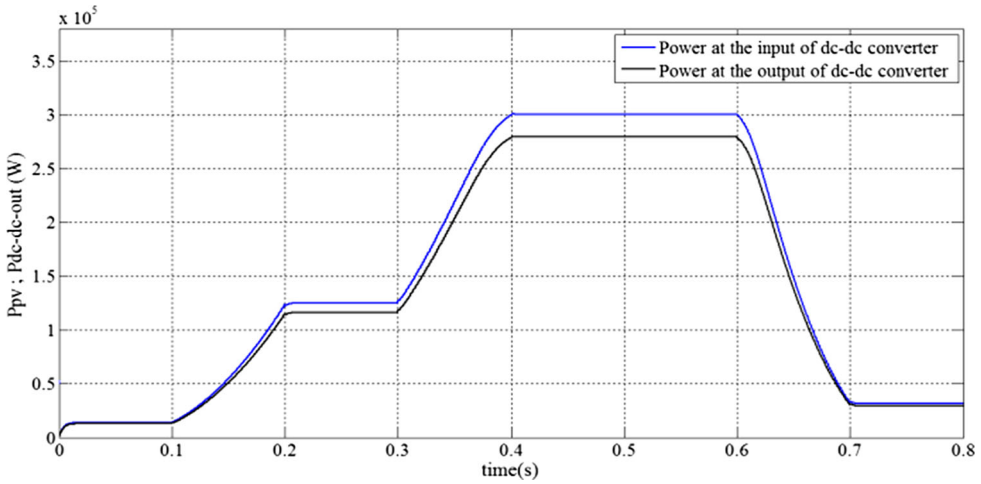

2.2.4 Membership function of FLC

The membership functions of fuzzy logic controller are shown in Fig. 8.

The MPPT using the Mamdani FLC approach, which uses the min–max operation fuzzy combination law, is designed in a manner that the control task tries to continuously move the operation point of the solar array as close as possible to the maximum power point (MPP), and the defuzzification uses the center of gravity method to compute the output of this FLC.

2.3 The three-phase nine levels NPC inverter model

Figure 9 shows the diagram of the three-phase nine levels NPC inverter with a capacitive divider at its input. It is com-

Author's personal copy

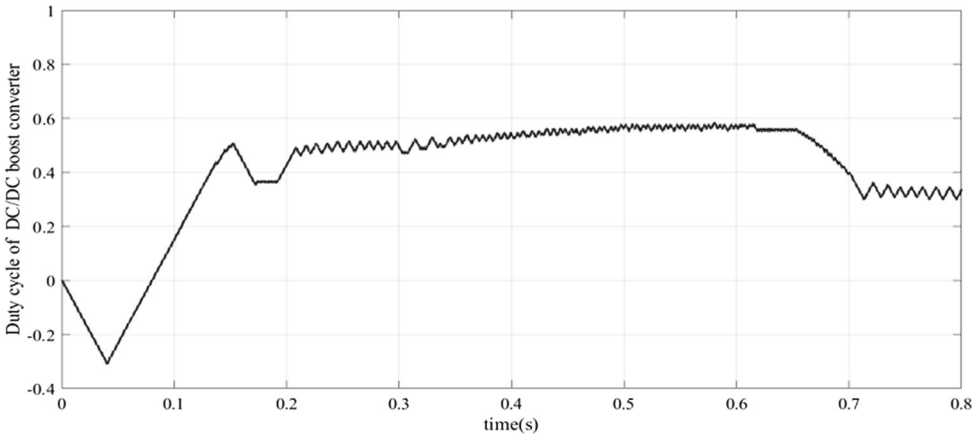

Fig. 19 Duty cycle of each DC/DC boost converter

posed of three arms; each one of them is composed of sixteen IGBTs that are noted as "S_{ij}." The index (i) indicates the phase: if i = 1, it means the phase "A," i = 2 the phase "B" and i = 3 the phase "C." The index (j) indicates the switches noted as: S_{i1}, S_{i2}, S_{i3}, S_{i4}, S_{i5}, S_{i6}, S_{i7}, and S_{i8} form the upper part of the arm in each phase and the switches noted as: S'_{i1}, S'_{i2}, S'_{i3}, S'_{i4}, S'_{i5}, S'_{i6}, S'_{i7}, and S'_{i8} form the lower part of the arm in each phase. Each arm of the inverter also comprises fourteen clamped diodes, which are denoted "D_{ij}." The output of the inverter is connected to the electric grid through a filter. The NPC inverter can generate 09 voltage levels: Four levels are positive, one level is zero, and four levels are negative. The NPC inverter is composed of 48 switches, hence the necessity de 48 control signals. These signals can be generated by a PWM controller.

2.4 Control circuit of the inverter

The control circuit of the inverter is shown in Fig. 10. It is based on the use of the PWM strategy in a closed-loop current. This strategy consists in comparing eight carrier signals of the same frequency (f_c = 400,Hz) with a sinusoidal reference signal. PI controllers are also used; they are characterized by their coefficients Ki and Kp (Ki = 0.01; Kp = 0.01). A square signal is added. As has already been mentioned, each arm of the inverter is composed of sixteen IGBTs, hence the necessity of sixteen control signals. So for these control signals, a small Matlab program is performed.

The states of the switches for generating the inverter output voltage "V_a" are shown in Table 1.

3 Simulation of the overall system

The diagram of the simulation is shown in Fig. 11.

The PV source is presented with the DC/DC converters as shown in Fig. 12.

For a variable solar radiation, the signal builder block is used to create a trapezoidal signal. So, the output signal of this block is given as follows (Fig. 13).

The output filter and the grid are shown in Fig. 14.

The simulation results are summarized as follows.

3.1 Characteristics of the PV source

The photovoltaic source consists of four (04) parts. Each part represents a photovoltaic generator consisting of N_P parallel branches (N_P = 50) each of which contains N_S modules in series (N_S = 80). The output voltage of each photovoltaic generator is (17.3 × 80 = 1384 V). This generator delivers an output current, which is given by: 4.34 × 50 = 217 A) (Fig. 15).

The MPP is obtained for (V_{MPP} = 1384 V, I_{MPP} = 217 A and P_{MPP} = 300 kW).

The characteristics of each photovoltaic generator with MPPT, under a variable solar radiation, are presented in Fig. 16.

The tracking of the maximum power point (MPP) using fuzzy logic is shown in Fig. 16, and with the use of the button (data cursor), the coordinates of the MPP,at 1000 W/m^2, are illustrated.

3.2 Parameters of the DC/DC converter for each part

Figure 17 shows the input and the output voltage for the dc/dc converter for each part.

The amplification voltage is very clear. The voltage value of 1384V, generated by each PV source (under 1000 W/m^2), becomes, according to equation (15) [12], equal to 3008V at the output of DC/DC converters in series.

$$\frac{V_{out}}{V_{in}} = \frac{1}{1-D} \tag{14}$$

(With duty cycle D=0.54).

Author's personal copy

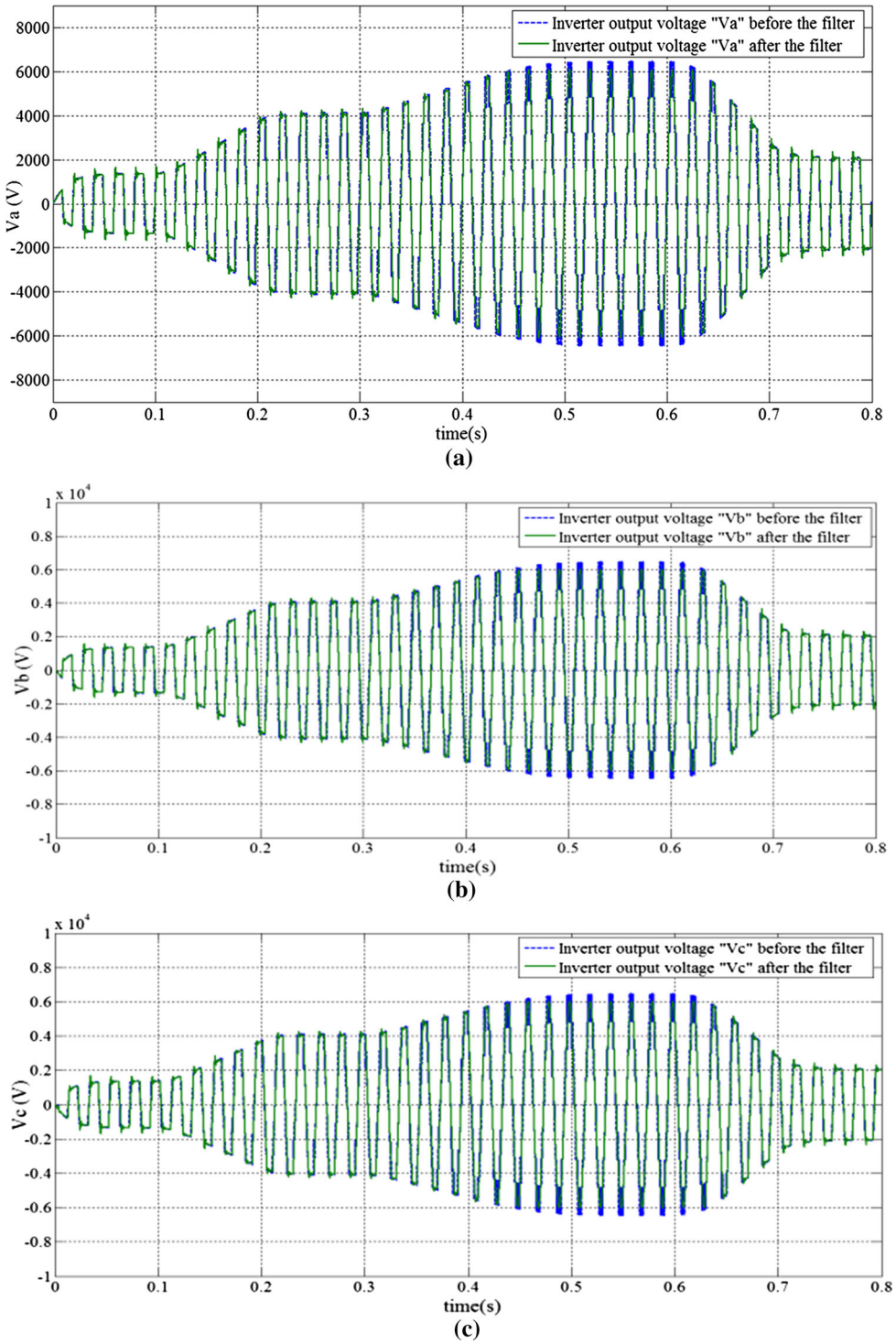

Fig. 20 Inverter output voltage before and after the filter: **a** Phase "a", **b** Phase "b", **c** Phase "c"

Figure 18 shows the input and the output power for the same converter:

3.3 Parameters of the NPC inverter

The duty cycle of each DC/DC boost converter is sketched in Fig. 19.

It is clear that the duty cycle varies with the intensity of the solar radiation. The results show that it reaches a value of 0.54 for 1000 W/m^2.

Figure 20 shows the voltages at the inverter output before and after the filter. For each phase, the voltage before filtering has a shape of a staircase waveform, with a maximum value (under 1000 W/m^2) of 6016 V $= V_{dc}/2$.

Author's personal copy

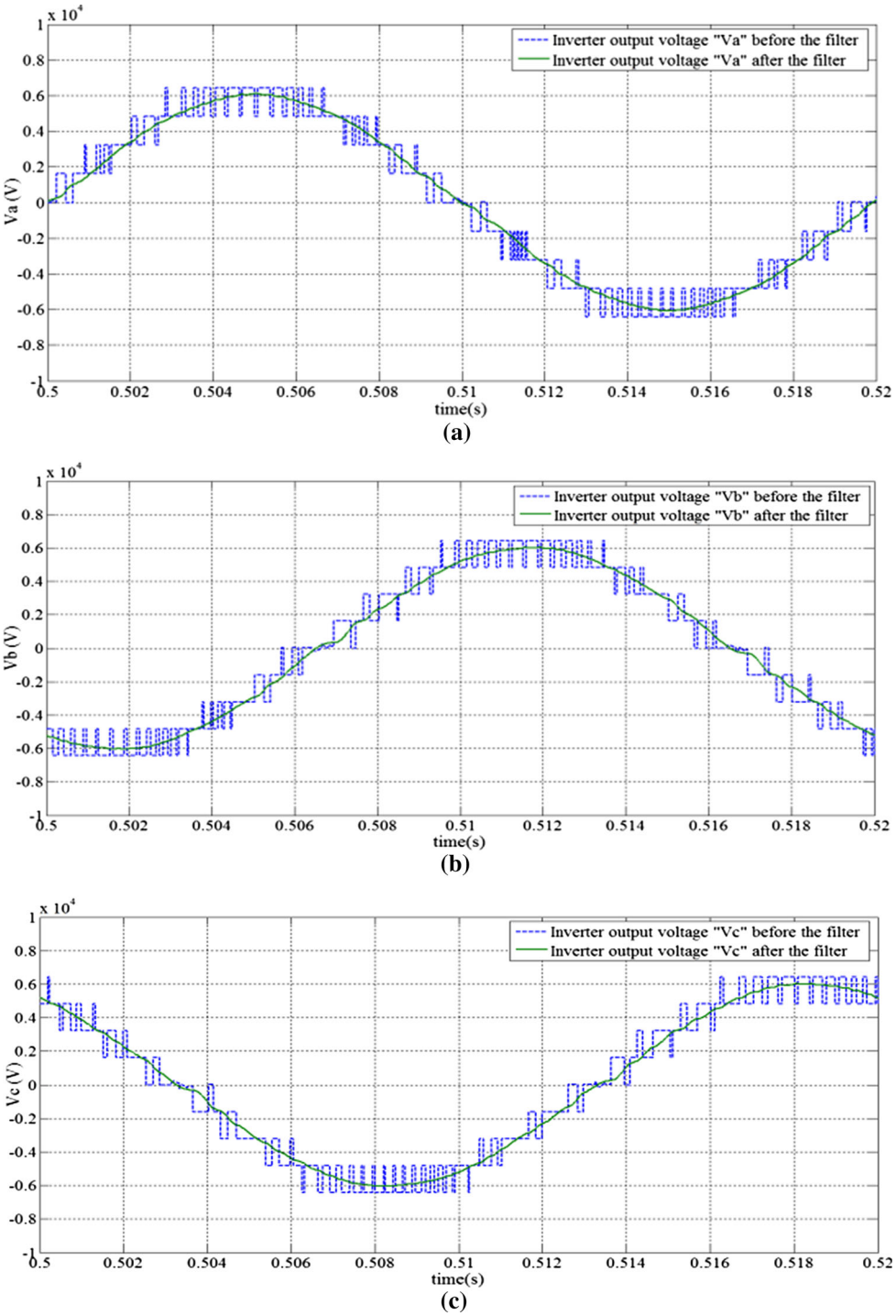

Fig. 21 One cycle of Inverter output voltage before and after the filter: **a** Phase "a", **b** Phase "b", **c** Phase "c"

However, the voltage after filtering becomes a sine wave that begins with a transitional phase of 0.03 s.

One period (for $0.50 < t < 0.52$) is illustrated in Fig. 21 for each phase:

The currents obtained before and after filtering at the output of the inverter are shown in Figs. 22 and 23.

One cycle of these currents is shown in Figs. 24 and 25.

The current shapes are sinusoidal with a substantially maximum value of 110 A.

When the grid is connected, the current wave forms are presented as follows.

Figures 26, 27, and 28 show the output current of the inverter for three phases "a," "b," and "c." It is obvious that in a radiation intensity ($G = 1000\,\mathrm{W/m^2}$) which is a high intensity, the output current after the filter is the

Author's personal copy

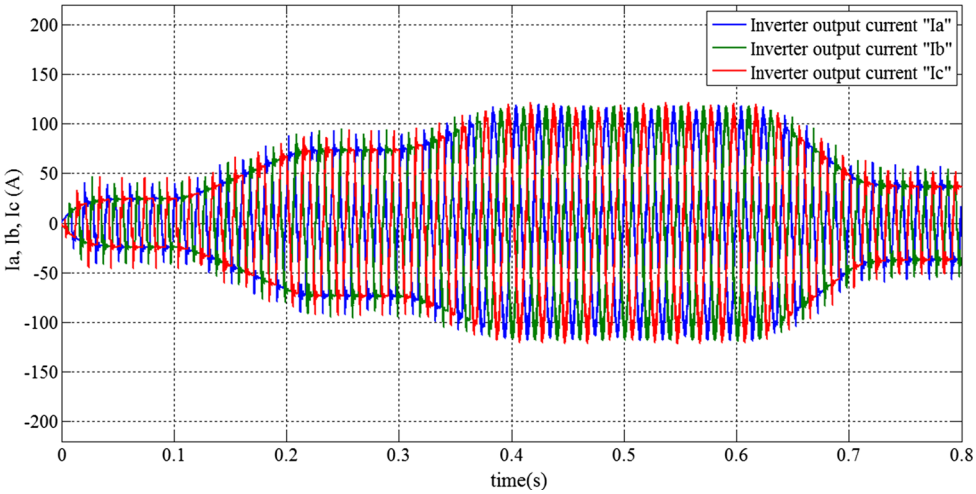

Fig. 22 Inverter output currents before the filter

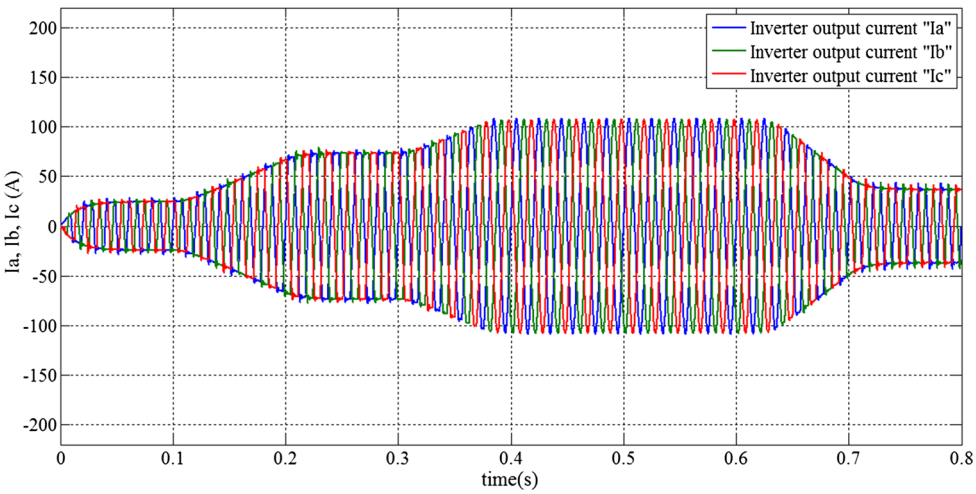

Fig. 23 Inverter output currents after the filter

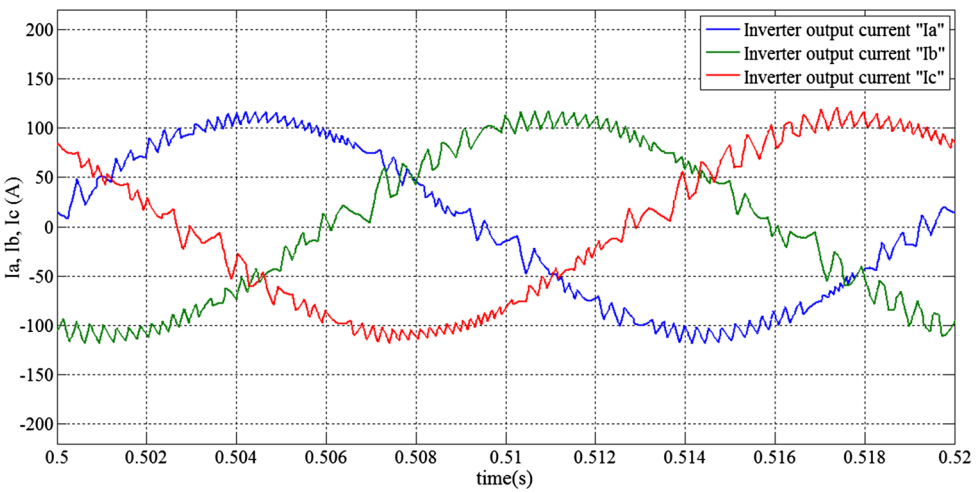

Fig. 24 One cycle of inverter output currents before the filter

Author's personal copy

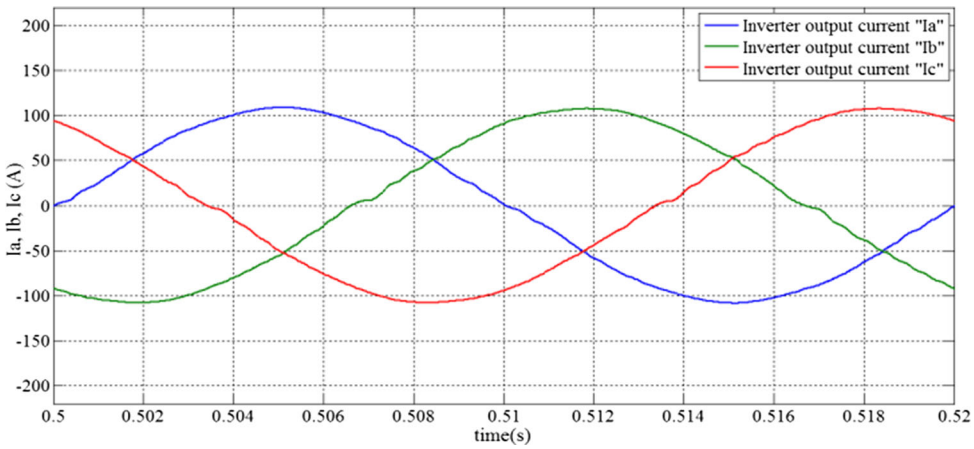

Fig. 25 One cycle of inverter output currents after the filter

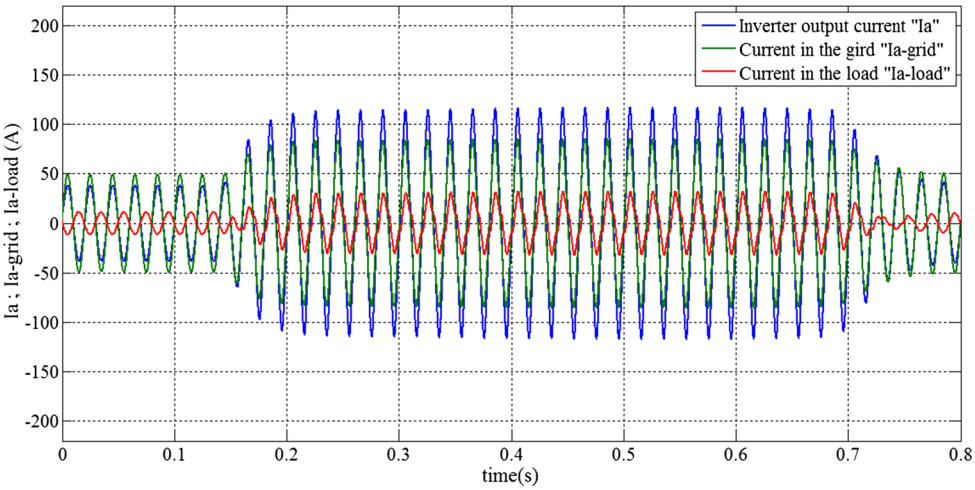

Fig. 26 Inverter output current for phase "a" (current after the filter I_{a}, current injected in the grid $I_{\mathrm{a-grid}}$ and current in the load $I_{\mathrm{a-load}}$)

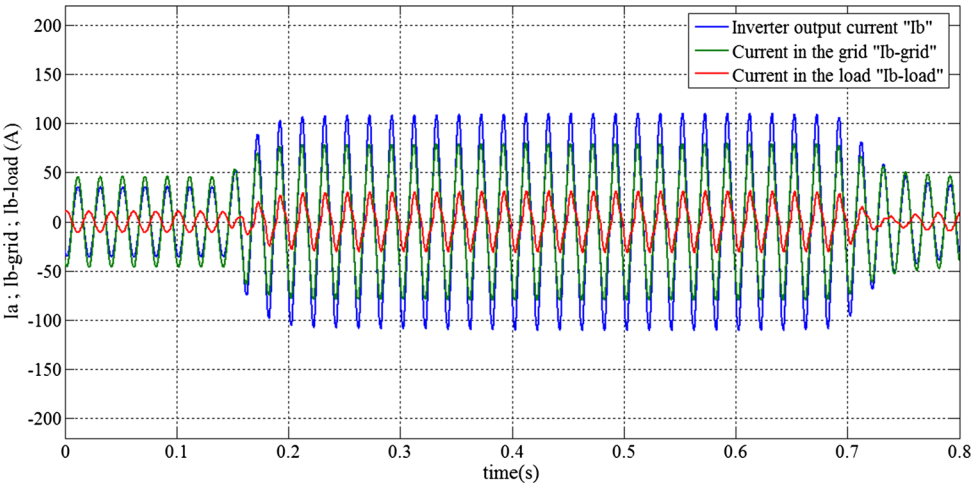

Fig. 27 Inverter output current for phase "b" (current after the filter I_{b}, current injected in the grid $I_{\mathrm{b-grid}}$ and current in the load $I_{\mathrm{b-load}}$)

Author's personal copy

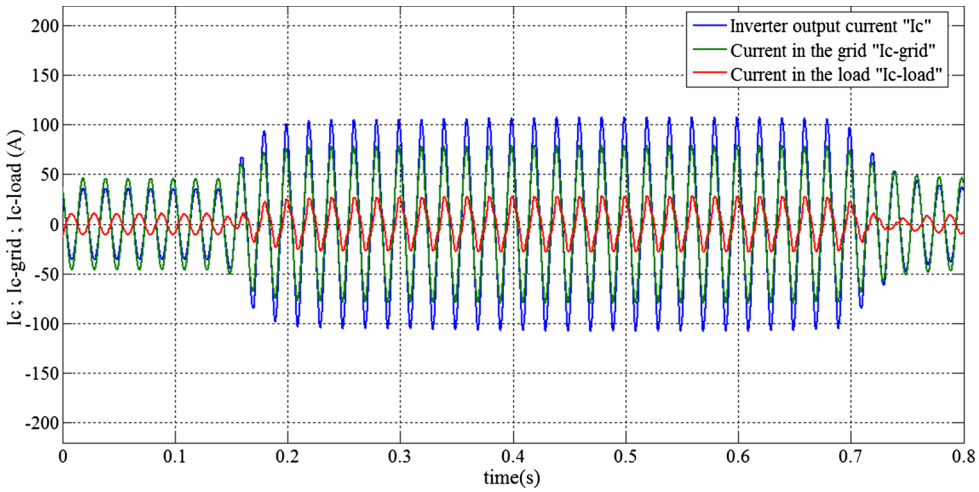

Fig. 28 Inverter output current for phase "c" (current after the filter I_c, current injected in the grid I_{c-grid} and current in the load I_{c-load})

sum of the current in the load and that injected in the grid.

Three cycles for the three-phase current, for a high intensity of the solar radiation, are illustrated in Fig. 29:

In case where phase "a" is taken as an example (see diagrams in Fig. 30), the currents in this phase are given by the Kirchhoff's law as follows:

$$I_a = I_{a-gird} + I_{a-load} \tag{15}$$

where I_a is the filtered inverter output current in phase "a," I_{a-grid} is the current in the grid, and I_{a-load} is the current in the load.

According to these results, we distinguish the two following cases:

a) First Case:

In this case, solar radiation is low (G<600W/m^2), if we consider the zoom in 0 <t <0.06 (see Fig. 30a).

We observe that it is the grid which feeds the load and there is a current which passes through the loop ①.

(b) *Second case*

In this case, solar radiation is high ($G > 600\,W/m^2$), and we clearly observe that it is the photovoltaic (PV) source that feeds the load and simultaneously injects a current into the grid (see Fig. 30b). We also observe that the increase in the intensity of the solar radiation results in an increase in the current at the output of the inverter and consequently an increase in the intensities of the currents in the load and in the grid

Therefore, to avoid the disturbances of the currents, it is necessary to connect the electric grid to the (PV) source under a constant solar radiation whose intensity is high (Fig. 31).

4 Conclusion

In this paper, the behavior of nine levels NPC three-phase inverter topology interfacing photovoltaic system to the medium electric grid under variable irradiance has been studied. Control of the NPC inverter was based on the PWM strategy which used eight carrier signals with different amplitudes, and with the same very low frequency of 0.4 kHz. MPPT fuzzy logic controller has been used, and it has been shown to perform well under variable irradiance. The connection of the (PV) system to the electrical grid must be made under constant and high solar radiation. The results are quite interesting. The efficiency of the inverter is very satisfying. However, the disadvantages of this system are the presence of a filter at the output, causing losses by Joule effect, and the use of multiple carrier signals for the control of the inverter. So to remedy this, it is preferable to use an inverter with more than nine levels in order to avoid the filter, and reduce the number of carrier signals in the control of the inverter. Also, the PV system requires a large number of solar modules with a power of 75 W which requires a large area to install, so it is preferable to replace them by more powerful solar modules.

In a future work, we can suggest firstly to change the inverter topology with only IGBTs, which reduces the number of switches in the inverter, secondly to choose a multioutput DC/DC converter instead of several converters DC/DC with a single output, and thirdly use this same topology with a hybrid renewable energy source.

Author's personal copy

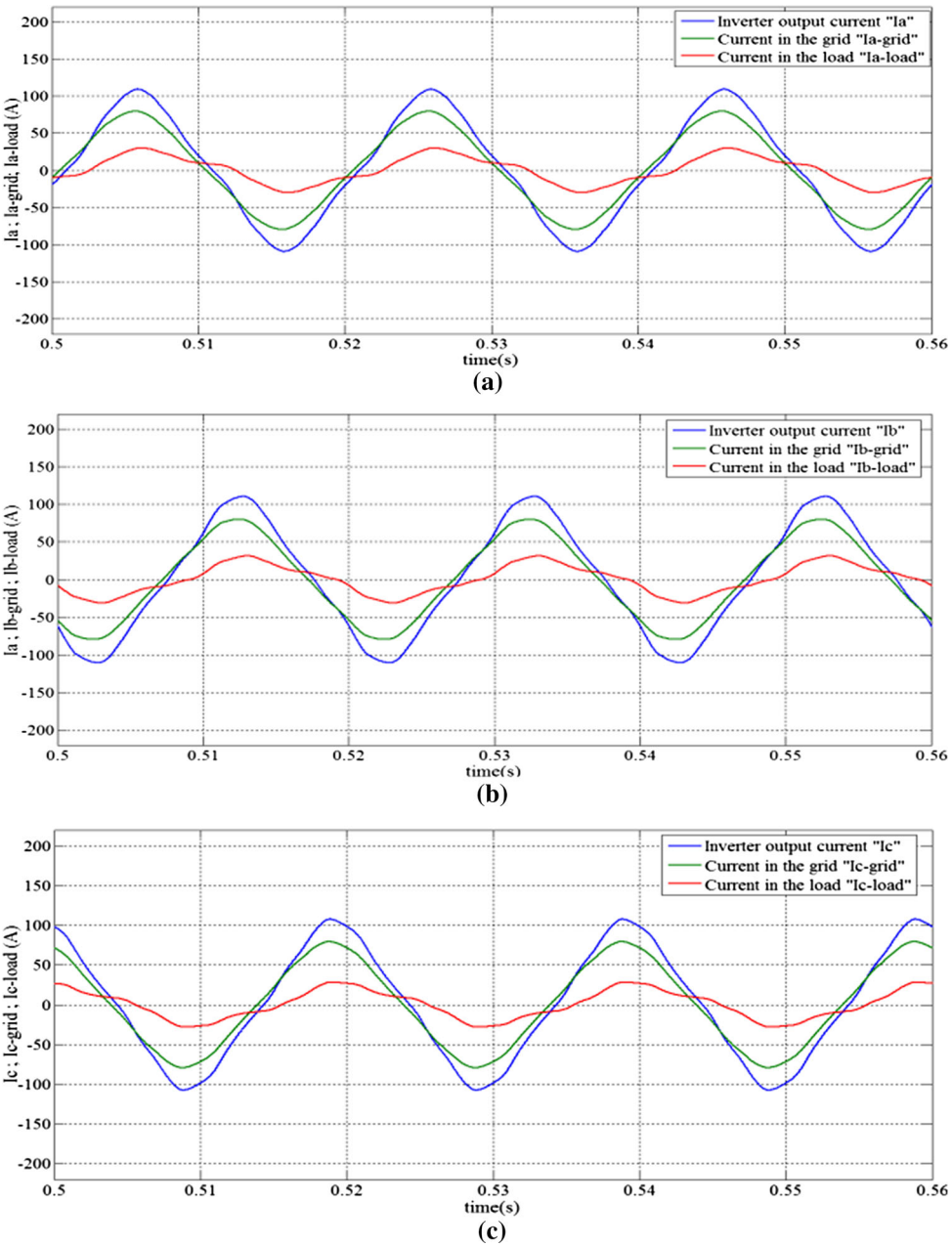

Fig. 29 Three cycles for the three-phase current (with grid connected, for $G = 1000\,\mathrm{W/m^2}$)

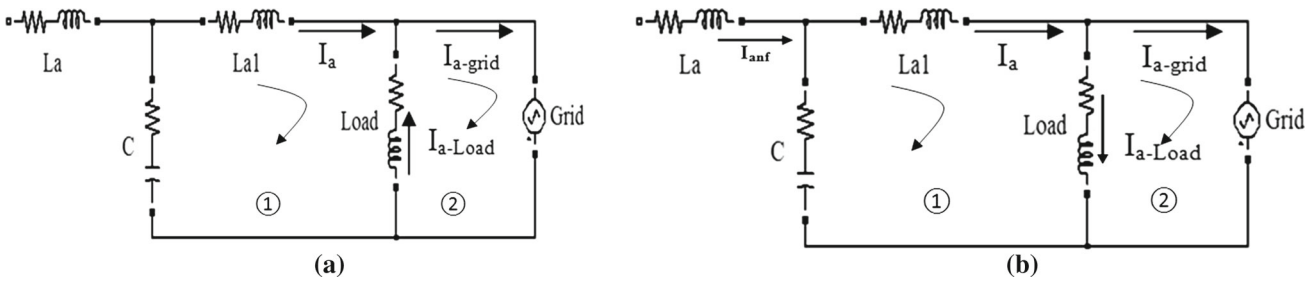

Fig. 30 Diagrams illustrating the directions of the currents in phase "a." **a** For low solar radiation, **b** for high solar radiation

Author's personal copy

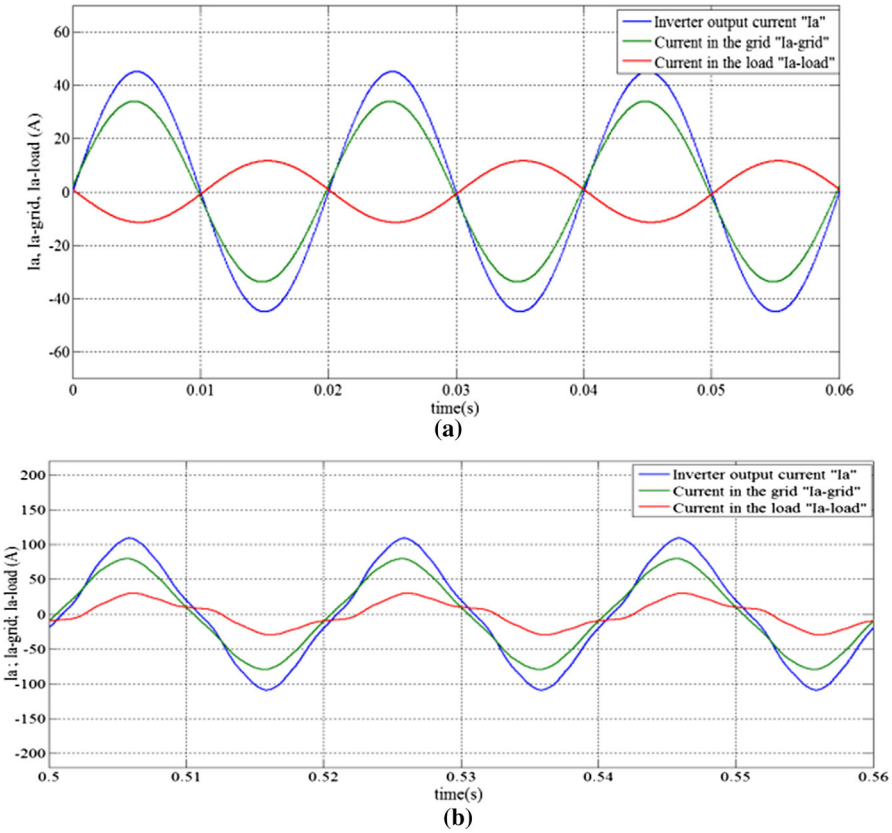

Fig. 31 Zoom of currents in phase "a". **a** Zoom in $0 < t < 0.06$s, **b** zoom in $0.5\,\text{s} < t < 0.56\,\text{s}$

Appendix

Parameters of ENIESOLAR module used in this work.

"ENIESOLAR" is a solar panel manufactured by the company National Electronic Industries in Algeria, which characteristics are given as follows:

Parameter	Value
Maximal power	75W, +/− 10%
Short-circuit current I_{SC}	4.67 A
Open-circuit voltage V_{OC}	21.6 V
MPP voltage V_{MPP}	17.30 V
MPP current I_{MPP}	4.34 A
Minimum value of the fuse in series	10 A
Number of cells in series	36
Number of cells in parallel	1

References

1. Vijay Kumar MG, Manjunath D, Patil Anil W (2012) Comparison of multilevel inverters with PWM control method. Int J IT Eng Appl Sci Res (IJIEASR) 1(3), ISSN: 2319-4413
2. Desconzi MI, Beltrame RC, Rech C, Schuch L, Hey HL (2010) Photovoltaic Stand-Alone Power Generation System with Multilevel Inverter. In: International Conference on Renewable Energies and Power Quality (ICREPQ'11), Las Palmas de Gran Canaria (Spain), 13th to 15th April
3. Jacobs IS, Bean CP. World energy statistics—2009. International Energy
4. Liserre M, Sauter T, Hung JY (2010) Future energy systems: integrating renewable energy sources into the smart power grid through industrial electronics. IEEE Ind Electron Mag 4(1):18–37
5. Hansen AD et al (2000) Models for standalone PV systems. Report Riso- R-1219(EN) SEC. RNL, Roskilde, Denmark
6. Castaner L, Silvester S (2002) Modeling photovoltaic systems using PSPICE. Wily, 1ère Édition ISBN 0-470-84528-7
7. Celik AN, Acikgoz N (2007) Modeling and experimental verification of the operating currents of mono-cristalline photovoltaic modules using four and five parameters models. Appl Energy 84(1):1–15
8. Marrakchi A, Kammoum S, Sallem S, Kammoum M (2015) A practical technique for connecting PV generator to single-phase grid. Sol Enegy 118:145–154
9. Graham D, Lathrop RC (1953) The synthesis of optimum transient response: criteria and standard forms. Trans Am Inst Electr Eng Part 2 Appl Ind 72(5):273–288
10. Terki A, Moussi A, Betka A, Terki N (2012) An improved efficiency of fuzzy logic control of PMBLDC for PV pumping system. Appl Math Model 36(3):934–944
11. Lee CC (1990) Fuzzy logic in control systems: fuzzy logic controller—parts I and II. IEEE Trans Syst Man Cybern 20(2):404–435
12. Mechouma Rabiaa, Azoui Boubekeur (2014) Multiple low frequency dual reference PWM control of a grid connected photovoltaic three phase NPC inverter with DC/DC boost converter. Serbian J Electr Eng (SJEE) 11(2):315–337